Robust Remaining Useful Lifetime Prediction for Lithium-Ion Batteries With Dual Gaussian Process Regression-Based Ensemble Strategies on Limited Sample Data

Xingjun Li, *Graduate Student Member, IEEE*, Dan Yu, *Graduate Student Member, IEEE*, Søren Byg Vilsen, *Member, IEEE*, Venkat R. Subramanian, *Member, IEEE*, and Daniel-Ioan Stroe, *Member, IEEE*

***Abstract*— Lithium-ion batteries have emerged as the primary power source for electric mobilities. Accurate remaining useful lifetime (RUL) prediction is required to ensure the safe operation of the batteries throughout their lifespan. This article proposes combination strategies that integrate two different Gaussian process regression (GPR) methods and model-based methods to enhance the robustness of the prediction. The first GPR is based on the forward extrapolation of the measured capacity sequence. The second GPR is based on the extrapolation of the measured feature and then inputs the predicted feature into a capacity estimation model. The first ensemble strategy is the weighted ensemble method, which uses the least squares method to determine the weighted coefficients. The second strategy is a more conservative method, which chooses the fastest degradation path between two basic methods at each prediction step. The third strategy is particle filter (PF), which combines the predicted data from different methods. The batteries aged by a real forklift aging profile and open access dataset are used to verify the proposed methods. The results of all methods based on different percentages of data are analyzed. The results show that individual methods may obtain different prediction results, while ensemble strategies have accurate and robust predictions. The PF for capacity-based and feature-based methods has the best performance with the absolute error of RUL less than 23 full equivalent cycles (FECs), error of prediction steps less than 1, and negligible simulation time for the forklift dataset.**

***Index Terms*— Ensemble learning, Gaussian process regression (GPR), lithium-ion batteries, remaining useful lifetime (RUL) prediction.**

Received 12 July 2024; revised 8 October 2024; accepted 15 November 2024. Date of publication 22 November 2024; date of current version 26 March 2025. This work was supported in part by the Otto Mønsteds Fond under Grant 23-70-2354, in part by the William Demant Foundation under Grant 23-4210, and in part by China Scholarship Council under Grant 202108320111 and Grant 202208320055. *(Corresponding author: Dan Yu.)*

Xingjun Li is with the Department of Energy, Aalborg University, 9220 Aalborg, Denmark, and also with the Walker Department of Mechanical Engineering, The University of Texas at Austin, Austin, TX 78712 USA (e-mail: xinli@energy.aau.dk).

Dan Yu and Daniel-Ioan Stroe are with the Department of Energy, Aalborg University, 9220 Aalborg, Denmark (e-mail: dayu@energy.aau.dk; dis@energy.aau.dk).

Søren Byg Vilsen is with the Department of Mathematical Sciences, Aalborg University, 9220 Aalborg, Denmark (e-mail: svilsen@math.aau.dk).

Venkat R. Subramanian is with the Walker Department of Mechanical Engineering, The University of Texas at Austin, Austin, TX 78712 USA (e-mail: venkat.subramanian@utexas.edu).

Digital Object Identifier 10.1109/TTE.2024.3504743

I. Introduction

ELECTRIC mobility applications, including electric vehicles, electric forklifts, and electric vertical take-off and landing vehicles, are emerging as replacements for internal combustion vehicles due to improvements in battery performance and reduced cost [1], [2], [3]. Lithium-ion batteries are the mainstream power sources in these applications because of their high power and energy density, high efficiency, and mature manufacturing process [4]. The capacity and power of lithium-ion batteries will, however, degrade under storage and operation conditions due to the loss of active material, and lithium inventory [5]; thus, state monitoring and management of batteries are essential to ensure their safe operation. Remaining useful lifetime (RUL) is an index used to evaluate the amount of time or number of cycles that the battery can operate from the present until it reaches the predefined end of life (EOL) criteria. Accurate, robust, and reliable RUL prediction can offer maintenance and/or replacement instructions and reduce the occurrence of battery accidents.

RUL prediction methods are usually divided into model-based, data-driven methods, and hybrid methods. The model-based methods include electrochemical models, equivalent circuit models, and empirical models. The key to the electrochemical model lies in coupling aging mechanisms, such as solid-electrolyte interphase and cathode-electrolyte interphase film growth [6], with electrochemical models like the pseudo two dimensions model [7], quasi-3-D model [8], and their reduced order models [9] to describe degradation trajectory. The challenges are to identify a lot of parameters by complex tests and be solved by a stable and fast solver. The computation of this method is intensive, and the result is unstable. Equivalent circuit models use electronic components to approximately describe the electrochemical characteristics of batteries [10]. It is simpler than electrochemical models. Its accuracy, however, is not higher, and parameter identification and coupling with the aging model are still inevitable. Empirical models usually build the relationship between the capacity and cycles according to the degradation trajectory,

and their parameters can be obtained by fitting methods [11], [12] or updated by filter algorithms [13], [14]. The common empirical models include the polynomial, dual exponential, and logarithmic models [15]; however, empirical models rely heavily on prior knowledge. The model accuracy will be very low when the measured aging trajectory is significantly different from the future trajectory [16]. Data-driven methods for RUL prediction have been extensively researched and can be broadly classified into EOL point prediction methods and sequence extrapolation methods [17]. EOL point prediction methods directly establish a mapping between features extracted from sampled data at the current cycle and the corresponding RUL using machine learning (ML) methods. For example, the difference in discharge capacity curves against voltage across different cycles was extracted from 124 batteries in [18] to predict the cycle life using a linear model, achieving a test error of 9.1% with the first 100 cycles. Yang et al. [19] investigated the importance of features related to RUL across different state of charge (SOC) ranges using random forest. These methods, however, require a large amount of test data to validate the effectiveness of the trained mapping. In contrast, sequence extrapolation methods are suitable for predicting the RUL of individual batteries or a limited number of batteries. These methods can be further categorized into sequence-to-sequence prediction and iterative sequence-to-point prediction. The input sequences can be either capacity sequences or feature sequences. In the sequence-to-sequence approach, past capacity or feature sequences are used as inputs to predict future capacity or feature sequences up until EOL using ML methods. When the output sequence consists of all the capacity or feature values from the current cycle to EOL, it is referred to as a one-shot prediction, as the prediction is performed in a single iteration, reducing computational time. A typical example of one-shot prediction was proposed by Li et al. [20], where the long short-term memory (LSTM) network with autoencoder and decoder methods was employed. The sequence-to-point prediction iteratively uses past capacity or feature sequences to predict a single capacity or feature value at each step until the EOL point is reached. The advantages of sequence-to-point methods include ease of implementation and reduced training data requirements; furthermore, capacity extrapolation means using the measured capacities to predict future capacity until reaching the EOL, where ML methods are used to learn the degradation trend in measured data. Liu et al. [21] proposed the LSTM optimized by an improved sparrow search algorithm to predict RUL, where the input was the capacity of the $1-n$ cycles and the output was the capacity of $n+1$ cycle. The feature extrapolation methods use the measured features to predict future features first and then input the predicted features into the capacity estimation model. The estimated capacity will be used for RUL calculation. Yao et al. [22] trained an extreme learning machine to map the relationship between cycle numbers and features, and the capacity was estimated by the relevance vector machine. The estimated capacity was compared with the failure threshold to obtain the final RUL results. Li et al. [23] fit the polynomial function for features and cycles and then input the predicted features into a Gaussian process regression (GPR) model to obtain the predicted capacity and the relevant RUL results. Strictly speaking, neither of the above two research belongs to the feature extrapolation method. Feature extrapolation method means using measured features to predict future features by ML directly; further, the performance difference, like the accuracy of the two methods is not clear. It is still difficult to decide which prediction results from the two methods are better and should be used. Hybrid methods leverage the strengths of both model-based and data-driven approaches. Typically, the process begins by decomposing the capacity series. Next, model-based and data-driven methods are applied to predict the different decomposed components, and finally, the prediction results are combined [24].

To improve the robustness of predicted RULs, some researchers chose to group batteries based on similarity criterion first and then use the transfer learning method to predict degradation trajectory for each subgroup [25], [26]. Others adopted ensemble strategies. Wang et al. [27] proposed a two-phase degradation model according to the change point, and the particle filter (PF) was used to update the parameters of two models. Their work implemented an ensemble from the time domain. Liu et al. [28] used the empirical mode decomposition method to decompose capacity data into mode functions and a residual, then applied LSTM and GPR models to predict the RUL from two kinds of data, respectively, and ensembled the results finally. A more common ensemble method is to use filter methods to integrate the predicted results from the empirical model and ML model. Yan et al. [29] used the Kalman filter to fuse the results by the polynomial model and support vector machine. Chen et al. [13] used PF to combine the estimated capacities from fifth-order polynomials and GPR. For this ensemble method, one model is regarded as a state variable, and another result is used as an observation variable [30]. The choice of observation variable is, however, not reliable and requires prior knowledge. Besides, the current research data are based on the full charging and discharging and take the discharge amount of each cycle as capacity. For example, the NASA dataset has around 175 capacity points, and the CALCE dataset has 800 capacity points [31]. In real life, it is difficult to obtain the capacity in each cycle and use it to predict RULs.

From the above introduction, it can be concluded that the research on RUL prediction considering feature sequence extrapolation is limited. The prediction performance comparison and ensemble of capacity and feature extrapolation have rarely been reported. Most research is based on a large amount of sample points. This article, therefore, proposes and compares capacity and feature-based GPR prediction methods based on the different percentages of limited data from the forklift aging profile. Then, the ensemble strategies for these two kinds of methods are introduced, i.e., the weighted least squares method, the conservative method, and the PF methods. Finally, the prediction accuracies of different single methods and ensemble strategies are compared, and the robust method is given.

The remainder of this article is organized as follows. Section II introduces the forklift aging data. Then, the two individual RUL prediction methods and the ensemble strategies are proposed in Section III. Next, Section IV presents and discusses the obtained results. Finally, the conclusions are summarized in Section V.

II. Description of Forklift Aging Data

A dataset for lithium-ion battery degradation based on a forklift mission profile, published recently by our group [32], was used to validate the proposed ensemble strategies for RUL prediction. Three prismatic lithium iron phosphate cells with a nominal capacity of 180 Ah were aged through the realistic and dynamic forklift mission profile at 35 °C, 40 °C, and 45 °C, corresponding to Cell 1, Cell 2, and Cell 3, respectively. The temperatures mentioned refer to the surface temperatures of the cells, measured by the thermocouples, which represent the actual operation temperatures. The thermal chambers were also set to 35 °C, 40 °C, and 45 °C (ambient temperatures). Because of the batteries' high thermal capacity, limited SOC variations, and precise control of the thermal chambers, temperature fluctuations within the cells were, however, minimal. The forklift mission profile was distilled from a four-month forklift field operation, and the whole current and voltage profiles are shown in Fig. 1(a) and (b), respectively. The whole profile accounts for approximately 23 full equivalent cycles (FECs) based on the initial capacity, and its SOC variation was the same as the real operation. The profile consists of multiple discharging and recharging steps. A sample of the current and voltage signals during the first discharging and subsequent recharging is shown in Fig. 1(c) and (d), respectively. The discharging part was random and not easy to control; however, the recharging current of each step was fixed to 24 A.

The whole forklift profile was repeated over 50 rounds. After each round, a reference performance test (RPT) at 25 °C was conducted to measure the real capacity. The capacity degradation curves of three cells are shown in Fig. 2. Missing values were filled using interpolation and marked with solid circles in Fig. 2. The number of interpolated points in Cell 1, Cell 2, and Cell 3 is 2, 2, and 3, respectively. The degradation trajectories of three cells during the initial 600 FECs were close. After that, Cell 3 degraded faster due to the higher operation temperature, while Cell 1 and Cell 2 degraded slowly, following very close degradation trajectories. More information about the battery parameters, test devices, and procedures can be found in [32] and [33].

III. Framework for Dual GPR-Based Ensemble Strategies

This section introduces the framework for dual GPR-based ensemble RUL prediction. The key to the proposed method is to ensemble RUL prediction results derived from forward-predicted RUL values based on capacity and feature sequence, respectively. The capacity-based and feature-based GPR RUL predictions will be presented in detail first. Then different strategies to ensemble prediction results from different methods will be elucidated.

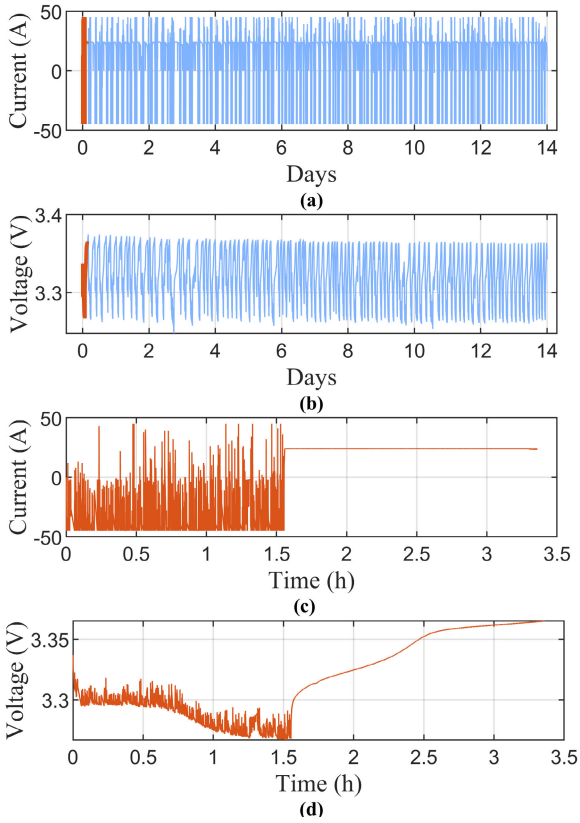

Fig. 1. Load profile of forklift used in Cell 1. (a) Current profile of one round of aging. (b) Voltage profile of one round of aging. (c) Current profile of Step 1 marked in (a). (d) Voltage profile of Step 1 marked in (b).

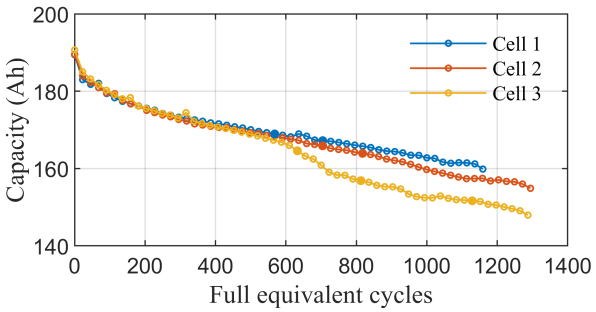

Fig. 2. Capacity degradation curves of three cells.

A. Capacity-Based GPR RUL Prediction

The capacity-based RUL prediction belongs to the sequence-to-point prediction method, which iteratively uses the measured capacity sequence to predict the capacity at the next FEC until the capacity reaches the EOL. The RUL is the difference between the FEC at EOL and the current FEC as

$$\mathrm{RUL} = \mathrm{FEC}_{\mathrm{EOL}} - \mathrm{FEC}_{\mathrm{now}} \tag{1}$$

where $\mathrm{FEC}_{\mathrm{EOL}}$ is the FEC at EOL. The capacity of $\mathrm{FEC}_{\mathrm{EOL}}$ reaches the predetermined lower limit. $\mathrm{FEC}_{\mathrm{now}}$ is the current FEC. In practice, the interval of FEC between two RPT sample points is usually not one, so the final RUL value is the multiplication of FEC interval (ΔFEC) between two RPTs and the number of forward prediction steps to EOL.

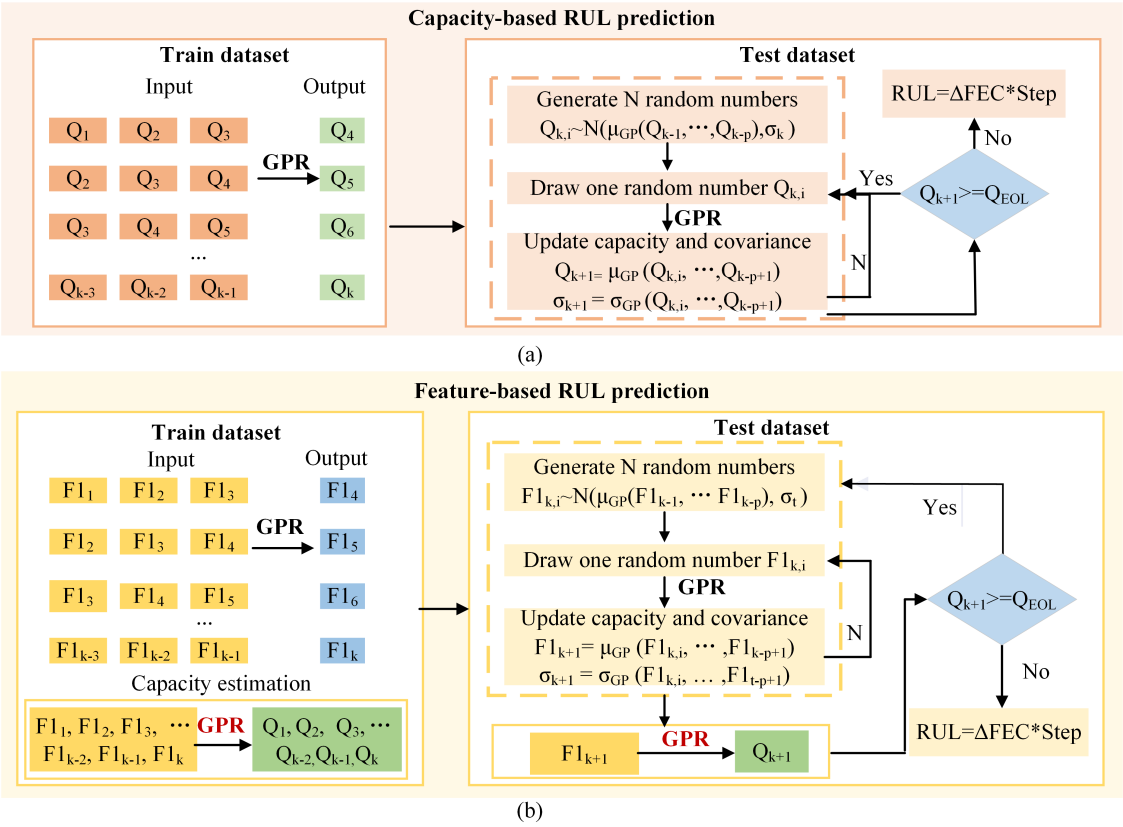

Fig. 3. Framework of capacity-based and feature-based prediction methods. (a) Capacity-based RUL prediction. (b) Feature-based RUL prediction.

In this case, the GPR method is used to map the relationship between the measured capacity sequence and the output point. The GPR is one nonparametric and Bayesian method that can provide predicted mean value and covariance simultaneously and can be expressed as

$$f(x) \sim GP\left(m(x), k\left(x, x'\right)\right) \tag{2}$$

where $f(x)$ is the predicted output, $m(x)$ is the mean function about FEC, $k(x, x')$ is the covariance function to reflect the variance of current FEC and covariance between different FECs. The covariance function is also called the "kernel function," which is the key to GPR and plays an important role in the prediction trajectory. The procedure of GPR is to use the observed samples to update and obtain the optimal parameters for the posterior mean and covariance function based on the prior mean and covariance function. The negative log marginal likelihood method is a common method. After preliminary trials, the linear kernel function was chosen in this work as

$$k_{\text{linear}}\left(x, x'\right) = x^T x'. \tag{3}$$

For the detailed mathematical derivation process of GPR, the reader is referred to [33].

In this work, the input sequence was composed of nine capacity values, and the output was the next capacity value. The sliding window size was one. Here, the two adjacent capacity values represented the value of two rounds of aging, and the FEC interval between them was approximately 23 FECs. The input and output data were fed into GPR to obtain the prediction model. N random numbers were generated to obtain the uncertainty in the prediction of the test dataset to represent the possible capacity values based on the predicted mean and covariance at each step. In the next prediction, one random number was drawn as the last value of the input sequence. The above procedure was repeated until the predicted capacity was less than the capacity at EOL. Finally, N possible capacity can be obtained in each step, and their mean values were regarded as the predicted capacities of this method. The flowchart of this method is described in Fig. 3(a).

B. Feature-Based GPR RUL Prediction

The approach of this method is to forward predict features based on the known data first, and then input the predicted feature into the capacity estimation model to obtain the future capacity and the RUL subsequently.

Specifically, one feature, i.e., the standard deviation of voltage curves during the first battery recharging, shown in Fig. 1(d), was first extracted. The recharging voltage curves of all rounds of Cell 1 are shown in Fig. 4.

The extracted features of the three cells are shown by dotted lines in Fig. 5(a). From Fig. 4, it can be seen that not all parts of the curve show the obvious aging evolution trend, and the voltage differences of Part II, is the most distinct. Nonuniform evolution trends of voltage curves led to the fluctuation and noise of the original extracted feature, which has a negative influence on the next feature prediction.

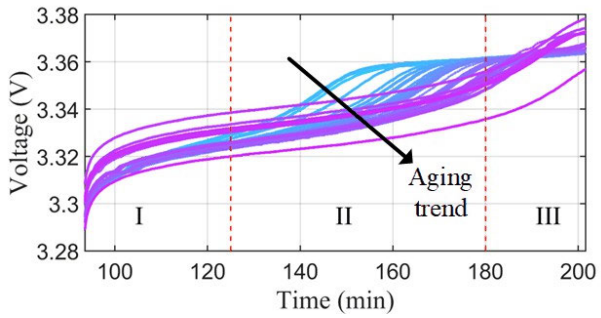

Fig. 4. Recharging voltage curves of Cell 1 in all rounds for feature extraction.

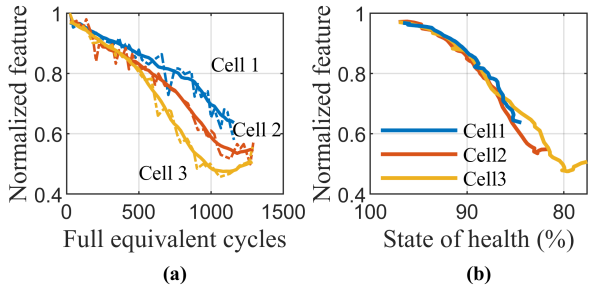

Fig. 5. Normalized features of three cells. (a) Original features and its MA filtered value. (b) Filtered features against the SOH.

The moving average (MA) method was, therefore, used to smooth the original feature for a better reflection of the degradation trend as shown by the solid line in Fig. 5(a). The Spearman coefficients between filtered and normalized features and capacity were −0.9987, −0.9948, and −0.9877, which show the strong monotonic relationship between them. Fig. 5(b) shows the relationship between the normalized feature and the state of health (SOH) of the three cells. The normalized feature decreases with the battery degradation. The three curves overlap when the SOH is larger than 85%, which makes it possible to use the aging data of Cell 2 and Cell 3 as the training set of the capacity estimation model for Cell 1. Additionally, the temperature for Cell 1 corresponds to the recommended operating temperature provided by the manufacturer.

Then, the known features were reconstructed as input and output sequences to train the GPR feature prediction model. The input sequence of the prediction model was the MA-smoothed and normalized feature extracted from the training dataset. Besides, the GPR estimation model mapping feature and capacity were built based on the known aging data. In the case of RUL prediction, the available data were only about the aging of the initial few cycles, where the degradation characteristics of the full cycle life cannot be fully described. Other similar cells with full cycle life data were, therefore, used to train the offline estimation model. Based on the trained feature prediction GPR model and capacity estimation GPR model, the feature of Cell 1 was predicted and then input into the estimation model to obtain the future capacity until EOL. The RUL was calculated by multiplying the FEC interval between each prediction step and the prediction steps to EOL. The method to generate uncertainty and possible predicted values in capacity-based GPR RUL prediction was also used to generate the possible features at each step. The mean of features at each step was input into the capacity estimation model to obtain the estimated capacity of this method. The flowchart of this method is described in Fig. 3(b).

C. Ensemble Strategies on Two Prediction Methods

The first ensemble strategy for the above two methods is the weighted least squares method. The predicted capacities from capacity-based and feature-based GPR methods were integrated through the weighted coefficients. The weighted coefficients were determined by the least squares method based on the predicted result and error in the training dataset. The principle was expressed as

$$\text{Minimize} \sum \left(w_1 * \hat{Q}_Q + w_2 * \hat{Q}_F - Q\right)^2 \tag{4}$$

$$\text{Subject to } w_1 + w_2 = 1 \tag{5}$$

where $\hat{Q}_Q$ is the predicted capacity using the capacity-based method in the training dataset, $\hat{Q}_F$ is the predicted capacity using feature-based capacity in the training dataset, Q is the real capacity, w_1 and w_2 are the corresponding weighted coefficients. Finally, the ensemble capacity is calculated as

$$\hat{Q}_{\text{weighted}} = w_1 * \hat{Q}_Q + w_2 * \hat{Q}_F \tag{6}$$

where $\hat{Q}_{\text{weighted}}$ is the ensemble capacity. Through this ensemble capacity, the robustness could be improved because the advantages of the two methods are considered. Overfitting is also more likely to occur because the weighted coefficients are, however, determined based on the training dataset.

The second ensemble strategy is called the "conservative method." In this method, the predicted capacities from two perspectives were compared at each prediction step, and the smaller of the two was regarded as the ensemble capacity, as expressed in

$$\hat{Q}_{\text{conservative},i} = \min\left(\hat{Q}_{Q,i}, \hat{Q}_{F,i}\right). \tag{7}$$

The smaller capacity means serious degradation and less RUL, and the conservative RUL can be obtained by this method.

The third ensemble strategy is PF. For the first ensemble strategy, the weighted coefficients are unchanged; however, these coefficients should be dynamic based on the prediction error at each step. PF can provide varying coefficients at each step. The essence of PF lies in using particles through Monto Carlo simulation to approximate recursive Bayesian filtering. In Bayesian filtering, the posterior probability of the state is calculated by multiplying the likelihood probability and the prior probability. PF employs weighted particles to represent the distribution of the posterior probability, making it a powerful tool for data fusion in nonlinear systems. The state-space equation of PF in this work is expressed as

$$\begin{cases} Q_k = f_1(Q_{k-1}, w_{k-1}) \\ y_k = f_2(Q_k, v_{k-1}) \end{cases} \tag{8}$$

where Q_k is the estimated capacity given by one method, and where y_k is the observed capacity, which is represented

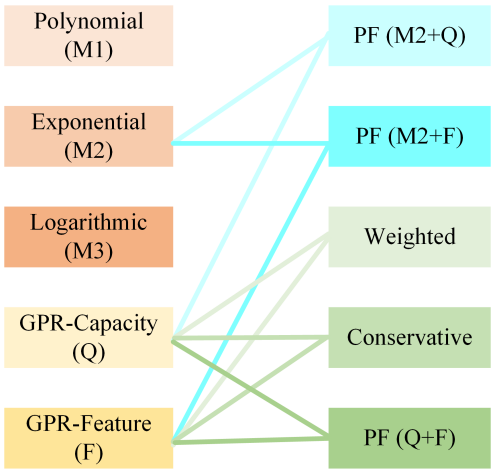

Fig. 6. All ensemble strategies in this work.

by another method. Through this method, two results are combined for robust capacity estimation and RUL prediction. The combined values are the mean of resampling particles. The procedure of PF includes four steps: 1) importance sampling, 2) weight calculation, 3) resampling, and 4) posteriori state approximation [34]. These steps are repeated until the EOL conditions are met.

For comparing the accuracy of more combinations, common empirical degradation models also acted as the base model. The three-order polynomial model (M1), dual exponential model (M2), and logarithmic model (M3) were expressed as

$$Q_k = p_1 k^3 + p_2 k^2 + p_3 k + p_4 \tag{9}$$

$$Q_k = a e^{bk} + c e^{dk} \tag{10}$$

$$\log(Q_k) = a_1 + b_1 k \tag{11}$$

where k is the FEC number, Q_k is the kth capacity. $p_1, p_2, p_3, p_4, a, b, c, d, a_1, b_1$ are the parameters, which are identified based on the known data. The empirical model, which has the highest prediction accuracy, will be combined with the ML model by PF for robustness. For the sake of space constraints and simplicity, only the third ensemble strategy was used to combine the empirical model and the ML model. All ensemble strategies are summarized in Fig. 6. After preliminary attempts, M2 has the highest accuracy in all cases. More details will be presented in Section IV.

D. Evaluation Metric

The prediction performance of proposed models and ensemble strategies was evaluated by the absolute error, relative error of the RUL, and capacity root-mean-square error (RMSE) as

$$\mathrm{AE_{RUL}} = |\mathrm{RUL_{real}} - \mathrm{RUL_{pre}}| \tag{12}$$

$$\mathrm{RE_{RUL}} = \frac{|\mathrm{RUL_{real}} - \mathrm{RUL_{pre}}|}{\mathrm{RUL_{real}}} \tag{13}$$

$$\mathrm{RMSE} = \sqrt{\frac{\sum_{i=1}^{i=N} \left(Q_i - \hat{Q}_i\right)^2}{N}} \tag{14}$$

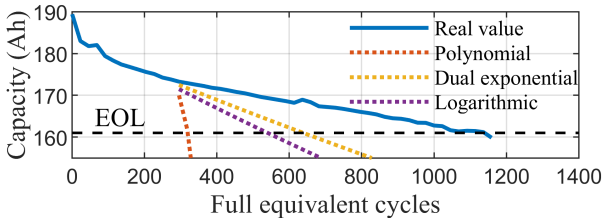

Fig. 7. RUL prediction results based on three empirical models using 25% aging data.

where $\mathrm{AE_{RUL}}$ is the absolute error of RUL, $\mathrm{RUL_{real}}$ is the real RUL, $\mathrm{RUL_{pre}}$ is the predicted RUL. $\mathrm{RE_{RUL}}$ is the absolute error of the predicted step. Q_i is the ith real capacity, and $\hat{Q}_i$ is ith predicted capacity. The ΔFEC at each prediction step was 22.72. The error of the prediction steps of the model ($\mathrm{AE_{RUL-step}}$) can be obtained by dividing the $\mathrm{AE_{RUL}}$ by ΔFEC

$$\mathrm{AE_{RUL-step}} = \frac{\mathrm{AE_{RUL}}}{\Delta \mathrm{FEC}} \tag{15}$$

where $\mathrm{AE_{RUL-step}}$ reflects the error between the real rounds number and predicted rounds number to EOL.

IV. Results and Discussion

In this work, Cell 1 was used as an example and test dataset to show the prediction results of the proposed methods. The aging data of Cell 2 and Cell 3 were used to train the capacity estimation model. 25%, 50%, and 75% of the aging data collected in Cell 1 were used for training the prediction model, individually. The RUL prediction results based on different percentages of aging data are presented and evaluated in this section.

A. RUL Prediction With 25% Aging Data

To research the RUL prediction performance of the proposed methods based on a small amount of measured data, 25% of the aging data (the first 13 rounds) were used as input for the prediction model. Fig. 7 shows the capacity prediction results of three empirical models. The capacity trajectories predicted by all three models deviated from the real value. The results from the double exponential model were relatively closer to the real values, so it was used to ensemble with GPR models.

Fig. 8 illustrates the prediction outcome using the capacity-based method. The results showed that this method was only effective during the initial prediction steps. Subsequent steps, however, revealed its limitation, characterized by a slow and nearly flat degradation curve.

On the contrary, the feature-based method demonstrated superior performance in this case, as shown in Fig. 9. The predicted features fit the real value in most steps. The uncertainty in most steps was narrow and gradually increased with aging. The estimated capacity in the training dataset was close to the real value with 1.3455 RMSE. Before the first 1000 FEC, the predicted capacity degradation trend was close to the real capacity degradation trend. After that, the capacity trajectory presented a slow increase trend due to the

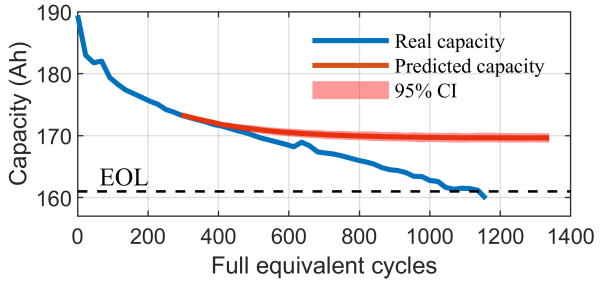

Fig. 8. RUL prediction results based on the capacity-based GPR method using 25% aging data.

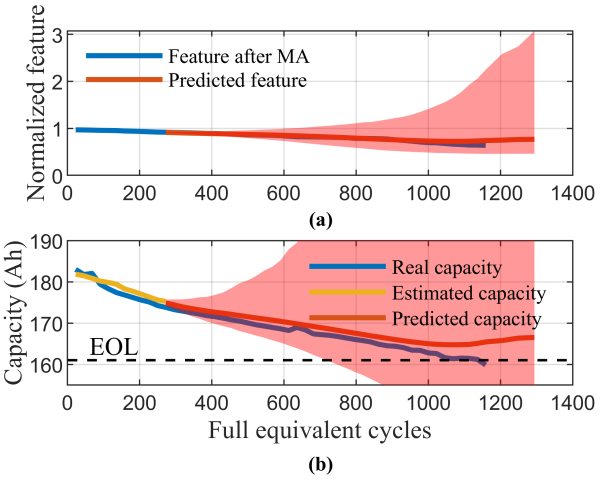

Fig. 9. Prediction results based on the feature-based GPR method using 25% aging data. (a) Feature prediction results with uncertainty. (b) Estimated and predicted capacities with uncertainty.

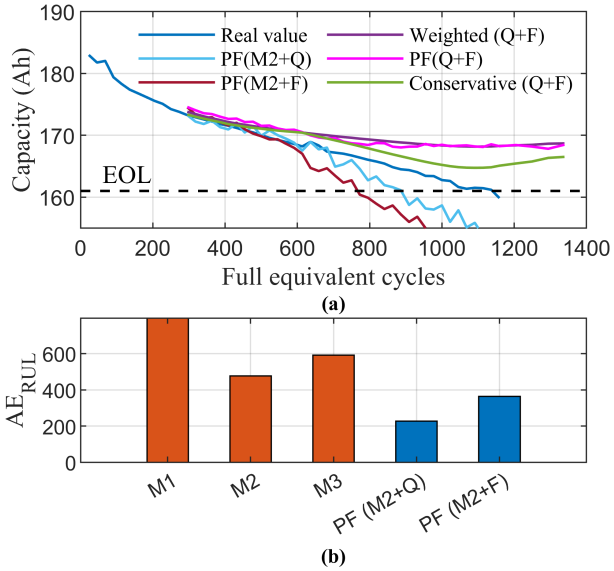

Fig. 10. Prediction results based on the ensemble strategies and the comparison of AE_{RUL} using 25% aging data. (a) Capacity prediction results and (b) comparison of AE_{RUL}.

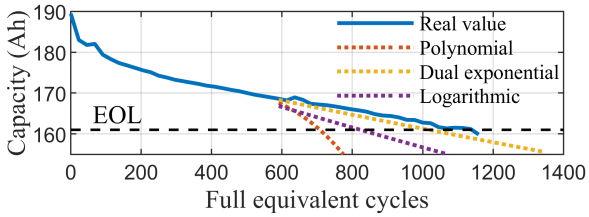

Fig. 11. RUL prediction results based on three empirical models using 50% aging data.

increase of the predicted features. The uncertainty interval of prediction also increased.

The ensemble prediction results using 25% of the aging data are presented in Fig. 10(a). The results of all ensemble strategies were far from the true values. The strategies that are model-based can capture the general trend. The values of the weighted method and PF for the capacity-based and feature-based methods were between the predictions of the two single methods and tended to lean toward the capacity-based method. For the conservative method, the predicted capacity by the capacity-based method was chosen before the first 600 FEC, and then that was feature-based capacity with 2.0960 RMSE. Fig. 10(b) shows the AE_{RUL} by strategies that can generate effective RUL predictions. The single model-based method has larger error. The PF strategies for model-based method with capacity-based and feature-based methods can reduce the AE_{RUL}.

B. RUL Prediction With 50% Aging Data

Only 50% of measured data (the first 26 rounds) were known and used to predict future capacities and RUL in this case. Fig. 11 shows the capacity prediction results by three empirical models. Only the dual exponential model closely fits the real value, where the corresponding predicted RUL and AE_{RUL} were 522.72 FECs and 45.59 FECs; therefore, the dual exponential model was further selected to combine with ML methods by PF. Fig. 12 shows the prediction results using the capacity-based GPR method. The mean of predicted capacities at each step was close to the actual value, but small fluctuations in actual values were not captured. The 95% confidence interval was narrow and could cover most of the real capacity. The real RUL and the mean of the predicted RUL were 568.32 FEC and 545.45 FEC, respectively. The AE_{RUL} and RE_{RUL} were 22.87% and 4%, respectively. The $AE_{RUL-step}$ based on the mean predicted RUL was 1.01. The distribution of $AE_{RUL-step}$ in 1000 randoms was counted and is shown as inset in Fig. 12. The statistics of the $AE_{RUL-step}$ less than 1 and 2 were 217 and 501, respectively, and the statics of the $AE_{RUL-step}$ less than 6 was 995, which shows higher prediction accuracy of this method.

Fig. 13 shows the prediction results by the feature-based GPR method. The predicted mean of features was not close to the real value at almost all prediction steps, and the confidence interval was very wide. After inputting the mean value of predicted features into the capacity estimation, it can be noted that the predicted capacity was close to the real value if the predicted feature was close to the real feature. The predicted RUL was 590.90 FEC and the corresponding AE_{RUL} and RE_{RUL} were 22.58 FEC and 3.9%, respectively. The $AE_{RUL-step}$ of this model was 0.99. This result was somewhat random because the predicted feature at EOL fit

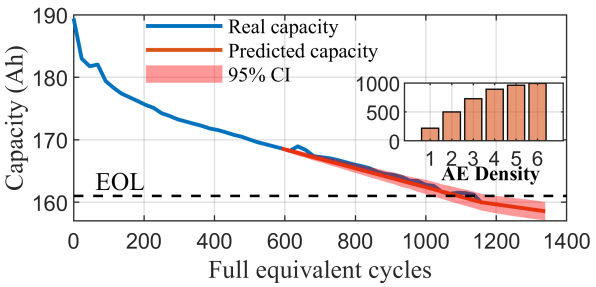

Fig. 12. RUL prediction results based on the capacity-based GPR method using 50% aging data. Inserted is the density of error of the prediction step.

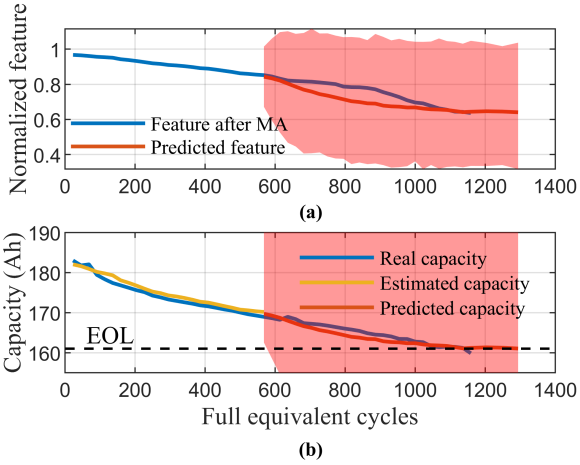

Fig. 13. Prediction results based on the feature-based GPR method using 50% aging data. (a) Feature prediction results with uncertainty. (b) Estimated and predicted capacities with uncertainty.

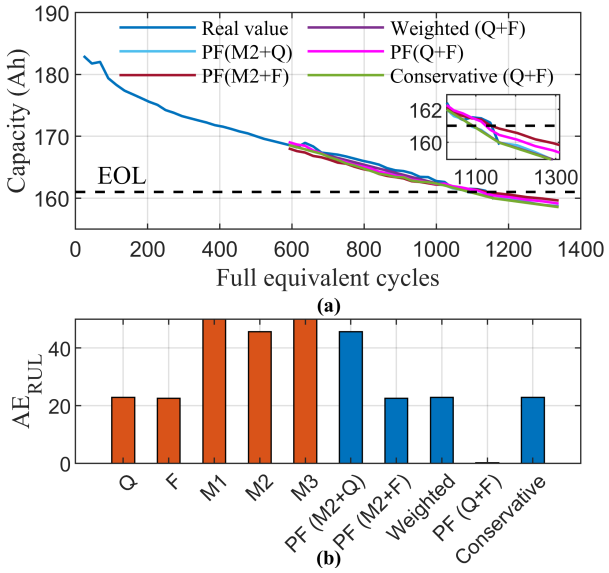

Fig. 14. Prediction results based on the ensemble strategies and the comparison of AERUL using 50% aging data. (a) Capacity prediction results. Inserted is the zoomed-in view around EOL. (b) Comparison of AE_{RUL}.

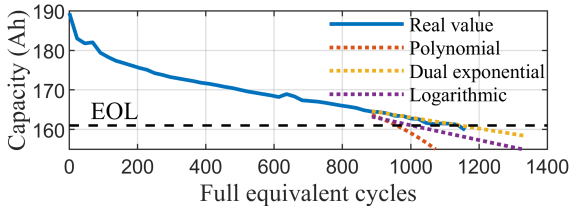

Fig. 15. RUL prediction results based on three empirical models using 75% aging data.

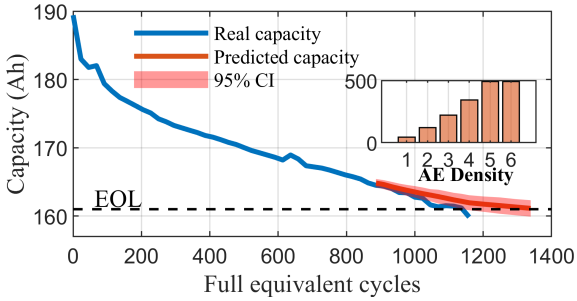

Fig. 16. RUL prediction results based on the capacity-based GPR method using 75% aging data. Inserted is the density of $AE_{RUL-step}$.

the real value well. The RMSE of the training dataset in the capacity estimation model was 1.06, which demonstrates the model can map the feature and capacity well.

From the analysis of Figs. 11 and 13, it can be found that the accuracy and robustness of a single method are not ideal in all prediction steps. Different ensemble strategies were, therefore, proposed, and the prediction results are shown in Fig. 14(a). All ensemble strategies fit well with the real value. Fig. 14(b) further summarized the AE_{RUL} of single methods (orange) and ensemble methods (blue). The AE_{RUL} of all ensemble strategies were less than 45.59 FECs i.e., 8% RE_{RUL}. The $AE_{RUL-step}$ was less than 2. Specifically, the AE_{RUL} of the strategy using PF to combine capacity-based GPR model and feature-based GPR model is 0.413, which is almost impossible to show in Fig. 14(b) due to the range of coordinates. Using the ensemble strategies can maintain and improve RUL prediction accuracy when 50% of aging data are available.

C. RUL Prediction With 75% Aging Data

This section presents the results of the proposed ensemble and single methods using a large amount of measured data, i.e., 75% of the data with 39 aging rounds. Fig. 15 illustrates the capacity prediction results by three empirical models. The predicted value from the three models were closer to the real value compared with using 25% and 50% of aging data. The results predicted by the dual exponential model were still the closest to the actual values. The corresponding RMSE and AE_{RUL} was 0.41 and 22.65, respectively. The dual exponential was used to further fuse.

Fig. 16 shows the capacity prediction outcome by the capacity-based method. The predicted capacity was slightly larger than the actual value, and the RMSE was 0.66. The mean of the predicted RUL was longer than the real value and AE_{RUL} was 113.56 FEC and $AE_{RUL-step}$ was 4.99. The uncertainty can cover the real value. As shown in the inset of Fig. 16, the number of $AE_{RUL-step}$ less than 1 to 5 was 43, 119, 221, 343, and 492, respectively, which means half of the predicted capacity points had $AE_{RUL-step}$ less than 5 compared to the actual value.

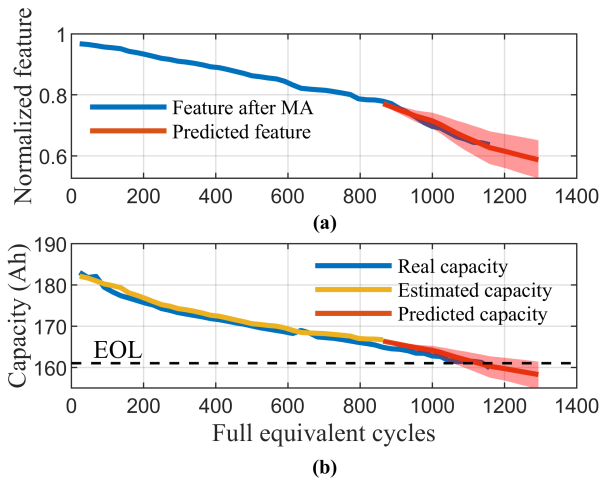

Fig. 17. Prediction results based on feature-based GPR method using 50% aging data. (a) Feature prediction results with uncertainty. (b) Estimated and predicted capacities with uncertainty.

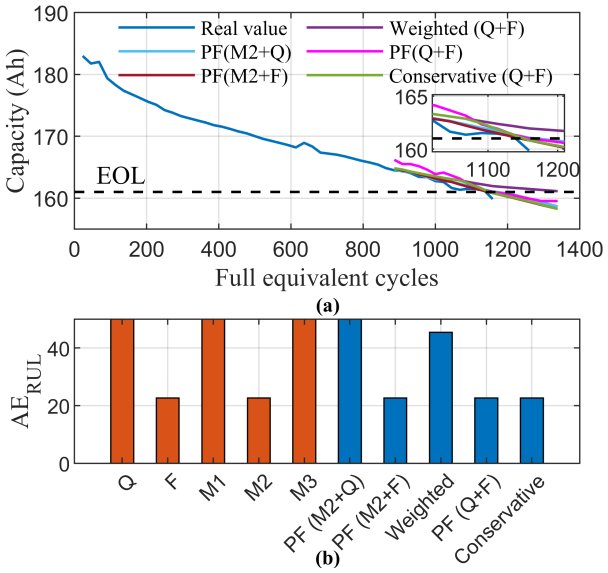

Fig. 18. Prediction results based on the ensemble strategies and the comparison of AE_{RUL} using 75% aging data. (a) Capacity prediction results. Inserted is the zoomed-in view around EOL. (b) Comparison of AE_{RUL}.

The prediction results by the feature-based method are shown in Fig. 17. The predicted features align well with the actual features with 0.0176 RMSE. Accordingly, the predicted capacities were close to real capacities with 1.4444 RMSE. The RMSE of estimated capacities in the training dataset was 1.0202. The AE_{RUL} and $AE_{RUL-step}$ were 22.65 FEC and 0.99, respectively. From the above results, the accuracy of the feature-based method was higher than that of using the capacity-based method.

The ensemble prediction results using 75% aging data are presented in Fig. 18(a). The prediction trajectory of the weighted strategy was similar to the capacity-based method, which has a longer RUL with 1.0190 RMSE. The performance of PF for capacity-based and feature-based models was poor in the initial steps of the prediction. The remaining ensemble strategies have similar prediction results. Fig. 18(b) summarizes the AE_{RUL} of all methods. The PF for the capacity-based and feature-based models and the conservative method can choose the single method with smaller errors from the two options.

D. Discussion and Comparison

From the above analysis, the prediction accuracy of the two single methods was not close all the time, especially when a reduced amount of data was used. It is necessary to ensemble two single methods for robust and accurate accuracy. Further, the predicted RUL and $AE_{RUL-step}$ of all single methods and ensemble strategies were summarized in Table I. Fig. 19 shows RMSEs of predicted capacity using different percentages of aging data based on all methods. It can be found that a single model was not enough for accurate RUL prediction in all cases. The prediction accuracy of model-based methods increases when the percentage of aging data increases. When a small amount of measured data is available, using PF to fuse model-based and ML-based methods can obtain predicted RUL with less error. For a medium and large amount of data case, PF for the capacity-based and feature-based methods is the best, as it has the lowest $AE_{RUL-step}$ and almost the lowest RMSE in all percentages of aging data. The feature-based method has a lower $AE_{RUL-step}$ compared with the capacity-based method when it comes to single methods and the ensemble method with the model-based method. Because each prediction step has 23 FECs, the RE_{RUL} of the case with a large amount of measured data will become relatively larger; therefore, the $AE_{RUL-step}$ is a more reasonable metric compared to RE_{RUL} to evaluate model performance. The impact of varying percentages of missing data on prediction accuracy was also examined. Missing data points were randomly selected, and interpolation methods were used to fill the missing values. For the capacity-based method, the RMSE values for missing data percentages of 0%, 10%, 20%, 30%, 40%, and 50% are 0.5434, 0.7346, 0.8749, 0.5327, 1.0914, and 1.2891, respectively. As shown, the RMSE increases slightly with a higher percentage of missing data, but all values remain within an acceptable range. For the feature-based method, partial data loss does not significantly affect accuracy due to the inclusion of data from other cells in the training process.

TABLE I
RUL PREDICTION RESULTS FOR DIFFERENT METHODS

Methods	25% (Predicted RUL/ $AE_{RUL-step}$)	50% (Predicted RUL/ $AE_{RUL-step}$)	75% (Predicted RUL/ $AE_{RUL-step}$)
GPR-Q	-	545.45/1.01	386.36/4.99
GPR-F	-	590.91/0.99	295.45/0.99
M1	68.18/35.01	159.01/18.01	113.64/7.00
M2	386.36/21.01	522.73/2.01	295.45/0.99
M3	272.73/26.01	272.72/13.01	159.09/5.00
PF(M2+Q)	636.36/10.01	522.72/2.01	318.18/1.99
PF(M2+F)	499.99/16.01	590.91/0.99	295.45/0.99
Weighted	-	545.45/1.01	386.36/4.99
PF(Q+F)	-	568.18/0.01	295.45/0.99
Conservative	-	545.45/1.01	295.45/0.99

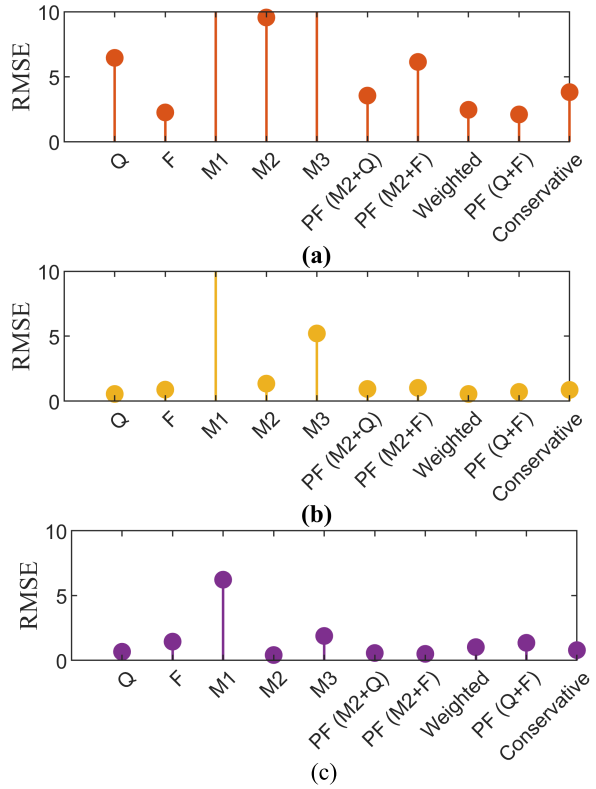

Fig. 19. RMSE comparison for different prediction methods using different percentages of aging data. (a) 25%, (b) 50%, and (c) 75%.

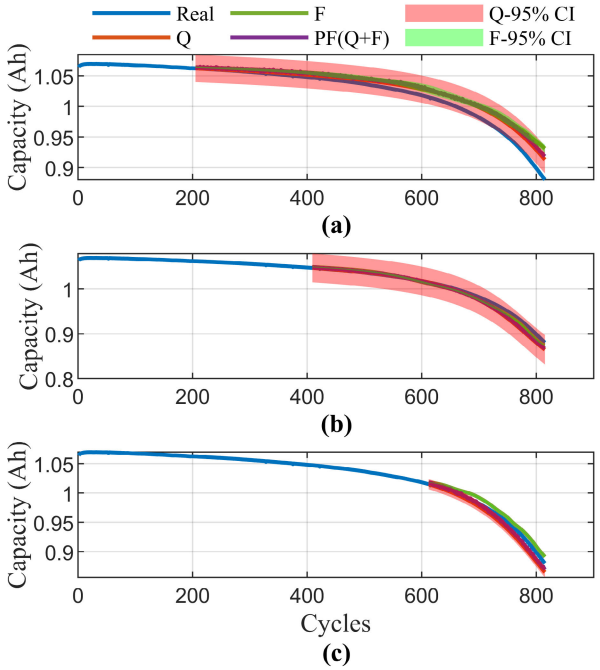

Fig. 20. Prediction results based on capacity-based GPR, feature-based GPR, and ensemble strategy (PF combination) using different percentages of the MIT dataset. (a) 25%, (b) 50%, and (c) 75%.

Additionally, to verify the generalization and effectiveness of the proposed methods on other data, different percentages of degradation data from two cells with the same aging profile (5.6 C(19%)-4.6 C) from the MIT dataset were used as input for the individual methods and the ensemble strategy (combining the capacity-based and feature-based methods using PF). The feature used in the feature-based method was the standard deviation of the incremental capacity during discharge (dQ/dV), where the same MA method was adopted to smooth the original feature before inputting. The prediction results using 25%, 50%, and 75% of aging data are shown in Fig. 20. All methods demonstrated the accurate prediction methods. For 25% of aging data, the RMSE values for the capacity-based, feature-based, and ensemble strategy were 0.0123, 0.0166, and 0.0148, respectively. For 50% of aging data, the RMSEs were 0.0086, 0.0054, and 0.0068, respectively. For 75% of aging data, the RMSEs were 0.0096, 0.0084, and 0.0065, respectively. The ensemble strategy can even achieve higher accuracy. As the input data increases, the confidence interval of predictions gradually narrows. The models are trained and performed well in all cases, as the selected cells had over 800 cycles, demonstrating the model's effectiveness and robustness in large sampling datasets.

The simulation times of different methods are summarized in Table II. The time of the feature-based method is larger than the capacity-based method due to the training of the estimation model. ML-based methods need more simulation time compared to model-based methods. All ensemble strategies do not require much time, and all of them are below 1 s. The more robust and accurate prediction results can be obtained without additional computational effort through ensemble strategies.

TABLE II
SIMULATION TIME FOR DIFFERENT METHODS

Single methods	Time (s)
GPR-Q	20.28
GPR-F	56.74
M1	0.06
M2	2.08
M3	0.16
Ensemble methods	**Time (s)**
PF(M2+Q)	0.09
PF(M2+F)	0.02
Weighted	0.99
PF(Q+F)	0.03
Conservative	0.01

The choice of state variable and observation variable for PF method influences prediction accuracy. For example, when the results from capacity-based model were used as state variable and those of feature-based model were used as observe variable, the AE_{RUL} was 0.1413. When they are changed, the AE_{RUL} was 22.58. The results from a more accurate method should be selected as the state variable.

The ML method used in this work was GPR not a neuron network-based method, because the sample data were limited, and the accuracy was acceptable.

V. CONCLUSION

Accurate, robust, and reliable RUL prediction of lithium-ion batteries is crucial for ensuring their safe operation. For enhancing the robustness of RUL prediction results, this

study proposes ensemble strategies for batteries aged by real and dynamic forklift aging profiles. Two distinct methods, the capacity-based forward prediction method and feature-based forward prediction method assisted by the capacity estimation model, are introduced. The weighted least squares, conservative, and PF methods are used to ensemble the predicted RUL results derived from two individual methods and empirical models. Different percentages of data were input to all proposed methods to evaluate their accuracy. The obtained results indicate that a single method cannot ensure accurate RUL prediction in all cases. The dual exponential model has the highest accuracy among all model-based methods. PF for model-based and ML-based methods can reduce the error of RUL prediction for 25% of the aging data cases. PF for capacity-based and feature-based methods is recommended for a medium and large amount of data case, where the AE_{RUL} and $AE_{RUL-step}$ is less than 23 FECs and 1 step in all cases with negligible computational cost. The feature-based method has higher accuracy compared with the capacity-based method when it comes to a single method and ensemble method with the model-based method, but the simulation time is longer. The proposed methods are still effective in other large sampling datasets. Future research will focus on data filtering, ensemble optimization, and comparison with electrochemical model-based prediction methods.

REFERENCES

[1] X. Lai et al., "Critical review of life cycle assessment of lithium-ion batteries for electric vehicles: A lifespan perspective," *eTransportation*, vol. 12, May 2022, Art. no. 100169, doi: 10.1016/j.etran.2022.100169.

[2] C. Liang, X. Xu, D. J. Auger, F. Wang, and S. Wang, "Efficient mode transition control for DM-PHEV with mechanical hysteresis based on piecewise affine H_∞ strategy," *IEEE Trans. Transport. Electrific.*, vol. 9, no. 3, pp. 4366–4379, Sep. 2023, doi: 10.1109/TTE.2023.3235012.

[3] M. Mitici, B. Hennink, M. Pavel, and J. Dong, "Prognostics for lithium-ion batteries for electric vertical take-off and landing aircraft using data-driven machine learning," *Energy AI*, vol. 12, Apr. 2023, Art. no. 100233, doi: 10.1016/j.egyai.2023.100233.

[4] L. Su, M. Wu, Z. Li, and J. Zhang, "Cycle life prediction of lithium-ion batteries based on data-driven methods," *eTransportation*, vol. 10, Nov. 2021, Art. no. 100137, doi: 10.1016/j.etran.2021.100137.

[5] C. Pastor-Fernández, T. F. Yu, W. D. Widanage, and J. Marco, "Critical review of non-invasive diagnosis techniques for quantification of degradation modes in lithium-ion batteries," *Renew. Sustain. Energy Rev.*, vol. 109, pp. 138–159, Jul. 2019, doi: 10.1016/j.rser.2019.03.060.

[6] W. Li, Z. Bao, Q. Gao, Q. Du, and K. Jiao, "Investigation of novel pulse preheating strategies for lithium-ion batteries at subzero temperature based on a multi-level CFD platform," *eTransportation*, vol. 19, Jan. 2024, Art. no. 100307, doi: 10.1016/j.etran.2023.100307.

[7] Y. Ren et al., "A data and physical model joint driven method for lithium-ion battery remaining useful life prediction under complex dynamic conditions," *J. Energy Storage*, vol. 79, Feb. 2024, Art. no. 110065, doi: 10.1016/j.est.2023.110065.

[8] W. Li, Q. Du, G. Guo, C. Wu, and K. Jiao, "Enhanced electrochemical and thermal behavior of lithium-ion batteries with ultrathick electrodes via oriented pores," *Appl. Thermal Eng.*, vol. 228, Jun. 2023, Art. no. 120555, doi: 10.1016/j.applthermaleng.2023.120555.

[9] L. K. K. Maia, L. Drünert, F. La Mantia, and E. Zondervan, "Expanding the lifetime of Li-ion batteries through optimization of charging profiles," *J. Cleaner Prod.*, vol. 225, pp. 928–938, Jul. 2019, doi: 10.1016/j.jclepro.2019.04.031.

[10] X. Jin, "Aging-aware optimal charging strategy for lithium-ion batteries: Considering aging status and electro-thermal-aging dynamics," *Electrochim. Acta*, vol. 407, Mar. 2022, Art. no. 139651, doi: 10.1016/j.electacta.2021.139651.

[11] S. Hong, C. Qin, X. Lai, Z. Meng, and H. Dai, "State-of-health estimation and remaining useful life prediction for lithium-ion batteries based on an improved particle filter algorithm," *J. Energy Storage*, vol. 64, Aug. 2023, Art. no. 107179, doi: 10.1016/j.est.2023.107179.

[12] D.-I. Stroe, M. Swierczynski, A.-I. Stan, R. Teodorescu, and S. J. Andreasen, "Accelerated lifetime testing methodology for lifetime estimation of lithium-ion batteries used in augmented wind power plants," *IEEE Trans. Ind. Appl.*, vol. 50, no. 6, pp. 4006–4017, Nov. 2014, doi: 10.1109/TIA.2014.2321028.

[13] D. Chen et al., "An empirical-data hybrid driven approach for remaining useful life prediction of lithium-ion batteries considering capacity diving," *Energy*, vol. 245, Apr. 2022, Art. no. 123222, doi: 10.1016/j.energy.2022.123222.

[14] Y.-H. Lin, L.-L. Tian, and Z.-Q. Ding, "Ensemble remaining useful life prediction for lithium-ion batteries with the fusion of historical and real-time degradation data," *IEEE Trans. Veh. Technol.*, vol. 72, no. 5, pp. 5934–5947, May 2023, doi: 10.1109/TVT.2023.3234159.

[15] J. Meng et al., "An empirical-informed model for the early degradation trajectory prediction of lithium-ion battery," *IEEE Trans. Energy Convers.*, vol. 39, no. 4, pp. 2299–2311, Dec. 2024, doi: 10.1109/TEC.2024.3385093.

[16] D. Yu, X. Li, S. S. Araya, S. L. Sahlin, and V. Liso, "Data-driven diagnosis of high temperature PEM fuel cells based on the electrochemical impedance spectroscopy: Robustness improvement and evaluation," *J. Energy Chem.*, vol. 96, pp. 544–558, Sep. 2024, doi: 10.1016/j.jechem.2024.05.014.

[17] X. Li, D. Yu, V. Søren Byg, and S. Daniel Ioan, "The development of machine learning-based remaining useful life prediction for lithium-ion batteries," *J. Energy Chem.*, vol. 82, pp. 103–121, Jul. 2023, doi: 10.1016/j.jechem.2023.03.026.

[18] K. A. Severson et al., "Data-driven prediction of battery cycle life before capacity degradation," *Nature Energy*, vol. 4, no. 5, pp. 383–391, 2019, doi: 10.1038/s41560-019-0356-8.

[19] N. Yang, H. Hofmann, J. Sun, and Z. Song, "Remaining useful life prediction of lithium-ion batteries with limited degradation history using random forest," *IEEE Trans. Transport. Electrific.*, vol. 10, no. 3, pp. 5049–5060, Sep. 2024, doi: 10.1109/TTE.2023.3323976.

[20] W. Li, N. Sengupta, P. Dechent, D. Howey, A. Annaswamy, and D. U. Sauer, "One-shot battery degradation trajectory prediction with deep learning," *J. Power Sources*, vol. 506, Sep. 2021, Art. no. 230024, doi: 10.1016/j.jpowsour.2021.230024.

[21] Y. Liu, J. Sun, Y. Shang, X. Zhang, S. Ren, and D. Wang, "A novel remaining useful life prediction method for lithium-ion battery based on long short-term memory network optimized by improved sparrow search algorithm," *J. Energy Storage*, vol. 61, May 2023, Art. no. 106645, doi: 10.1016/j.est.2023.106645.

[22] F. Yao, W. He, Y. Wu, F. Ding, and D. Meng, "Remaining useful life prediction of lithium-ion batteries using a hybrid model," *Energy*, vol. 248, Jun. 2022, Art. no. 123622, doi: 10.1016/j.energy.2022.123622.

[23] X. Li, C. Yuan, and Z. Wang, "Multi-time-scale framework for prognostic health condition of lithium battery using modified Gaussian process regression and nonlinear regression," *J. Power Sources*, vol. 467, Aug. 2020, Art. no. 228358, doi: 10.1016/j.jpowsour.2020.228358.

[24] Y. Chang, H. Fang, and Y. Zhang, "A new hybrid method for the prediction of the remaining useful life of a lithium-ion battery," *Appl. Energy*, vol. 206, pp. 1564–1578, Nov. 2017, doi: 10.1016/j.apenergy.2017.09.106.

[25] Y. Guo, Y. Wang, P. Ding, and K. Huang, "Future degradation trajectory prediction of lithium-ion battery based on a three-step similarity evaluation criterion for battery selection and transfer learning," *J. Energy Storage*, vol. 72, Nov. 2023, Art. no. 108763, doi: 10.1016/j.est.2023.108763.

[26] Y. Che, Y. Zheng, F. E. Forest, X. Sui, X. Hu, and R. Teodorescu, "Predictive health assessment for lithium-ion batteries with probabilistic degradation prediction and accelerating aging detection," *Rel. Eng. Syst. Saf.*, vol. 241, Jan. 2024, Art. no. 109603, doi: 10.1016/j.ress.2023.109603.

[27] R. Wang, M. Zhu, X. Zhang, and H. Pham, "Lithium-ion battery remaining useful life prediction using a two-phase degradation model with a dynamic change point," *J. Energy Storage*, vol. 59, Mar. 2023, Art. no. 106457, doi: 10.1016/j.est.2022.106457.

[28] K. Liu, Y. Shang, Q. Ouyang, and W. D. Widanage, "A data-driven approach with uncertainty quantification for predicting future capacities and remaining useful life of lithium-ion battery," *IEEE Trans. Ind. Electron.*, vol. 68, no. 4, pp. 3170–3180, Apr. 2021, doi: 10.1109/TIE.2020.2973876.

[29] L. Yan et al., "A hybrid method with cascaded structure for early-stage remaining useful life prediction of lithium-ion battery," *Energy*, vol. 243, Mar. 2022, Art. no. 123038, doi: 10.1016/j.energy.2021.123038.

[30] L. Chen, Y. Ding, B. Liu, S. Wu, Y. Wang, and H. Pan, "Remaining useful life prediction of lithium-ion battery using a novel particle filter framework with grey neural network," *Energy*, vol. 244, Apr. 2022, Art. no. 122581, doi: 10.1016/j.energy.2021.122581.

[31] B. Zraibi, C. Okar, H. Chaoui, and M. Mansouri, "Remaining useful life assessment for lithium-ion batteries using CNN-LSTM-DNN hybrid method," *IEEE Trans. Veh. Technol.*, vol. 70, no. 5, pp. 4252–4261, May 2021, doi: 10.1109/TVT.2021.3071622.

[32] S. B. Vilsen and D.-I. Stroe, "Dataset of lithium-ion battery degradation based on a forklift mission profile for state-of-health estimation and lifetime prediction," *Data Brief*, vol. 52, Feb. 2024, Art. no. 109861, doi: 10.1016/j.dib.2023.109861.

[33] X. Li, D. Yu, S. B. Vilsen, and D. I. Stroe, "Accuracy comparison and improvement for state of health estimation of lithium-ion battery based on random partial recharges and feature engineering," *J. Energy Chem.*, vol. 92, pp. 591–604, May 2024, doi: 10.1016/j.jechem.2024.01.037.

[34] X. Li, C. Yuan, Z. Wang, J. He, and S. Yu, "Lithium battery state-of-health estimation and remaining useful lifetime prediction based on non-parametric aging model and particle filter algorithm," *eTransportation*, vol. 11, Feb. 2022, Art. no. 100156, doi: 10.1016/j.etran.2022.100156.

Xingjun Li (Graduate Student Member, IEEE) received the B.E. and M.S. degrees in power engineering from Jiangsu University, Zhenjiang, China, in 2018 and 2021, respectively. He is currently pursuing the Ph.D. degree with the Department of Energy, Aalborg University, Aalborg, Denmark.

His research interests include state estimation, lifetime prediction, charging optimization, electrochemical modeling, and fault diagnostics for batteries.

Dan Yu (Graduate Student Member, IEEE) received the B.E. and M.S. degrees in power engineering from Jiangsu University, Zhenjiang, China, in 2018 and 2021, respectively. She is currently pursuing the Ph.D. degree with the Department of Energy, Aalborg University, Aalborg, Denmark.

Her research interests include machine learning-based state estimation and fault diagnostics for batteries and fuel cells.

Søren Byg Vilsen (Member, IEEE) received the B.Sc. degree in mathematics, the M.Sc. degree in applied mathematics, and the Ph.D. degree in statistics from Aalborg University, Aalborg, Denmark, in 2013, 2015, and 2018, respectively.

He is currently an Assistant Professor with the Department of Mathematical Sciences working closely with the Batteries Research Group, AAU Energy, Aalborg. His current research interests include statistical learning, evolutionary computation, deep learning, and sequential models with application to lithium-based battery state estimation and lifetime prediction.

Venkat R. Subramanian (Member, IEEE) received the B.E. degree in chemical and electrochemical engineering from the Central Electrochemical Research Institute, Karaikudi, India, in 1997, and the Ph.D. degree in chemical engineering from the University of South Carolina, Columbia, SC, USA, in 2001.

From 2014 to 2019, he was a Professor at the University of Washington, Seattle, WA, USA. He is currently a Professor with the University of Texas at Austin, Austin, TX, USA. His research interests include electrochemical modeling, nonlinear model predictive control, and model reformulation for batteries.

Daniel-Ioan Stroe (Member, IEEE) received the Dipl.-Ing. degree in automatics from the Transilvania University of Brasov, Braşov, Romania, in 2008, and the M.Sc. degree in wind power systems and the Ph.D. degree in lifetime modeling of lithium-ion batteries from Aalborg University (AAU), Aalborg, Denmark, in 2010 and 2014, respectively.

He was a Visiting Researcher with RWTH Aachen, Aachen, Germany, in 2013. He is currently an Associate Professor with AAU Energy, Aalborg, where he leads the Batteries Research Group and the Battery Systems Testing Laboratory. He has co-authored more than 150 journals and conference papers in various battery-related topics. His current research interests include the area of energy storage systems for grid and e-mobility, lithium-based batteries testing, modeling, diagnostics, and their lifetime estimation.